Low Temperature Physics/Fizika Nizkikh Temperatur, 2013, v. 39, No. 7, pp. 806–813

Dielectric properties of (CuO,CaO_2, and BaO)$_y$/CuTl-1223 composites

M. Mumtaz[1], M. Kamran[1], K. Nadeem[1], Abdul Jabbar[1],
Nawazish A. Khan[2], Abida Saleem[3], S. Tajammul Hussain[3], and M. Kamran[4]

[1]*Materials Research Laboratory, Department of Physics, International Islamic University (IIU), Islamabad 44000, Pakistan*
E-mail: mmumtaz75@yahoo.com

[2]*Materials Science Laboratory, Department of Physics, Quaid-i-Azam University (QAU), Islamabad 45320, Pakistan*

[3]*Nano Science & Catalysis Division, National Center for Physics*
Shadhara Valley Road, Quaid-i-Azam University Campus, Islamabad 45320, Pakistan

[4]*Department of Physics, COMSATS Institute of Information Technology Islamabad, Pakistan*

Received November 19, 2012, revised February 3, 2013

We synthesized (CuO, CaO_2, and BaO)$_y$/$Cu_{0.5}Tl_{0.5}Ba_2Ca_2Cu_3O_{10-\delta}$ (y = 0, 5%, 10%, 15%) composites by solid-state reaction and characterized by x-ray diffraction, scanning electron microscopy, dc-resistivity, and Fourier transform infrared spectroscopy. Frequency and temperature dependent dielectric properties such as real and imaginary part of dielectric constant, dielectric loss, and ac-conductivity of these composites are studied by capacitance and conductance measurement as a function of frequency (10 kHz to 10 MHz) and temperature (78 to 300 K). The x-ray diffraction analysis reveals that the characteristic behavior of $Cu_{0.5}Tl_{0.5}Ba_2Ca_2Cu_3O_{10-\delta}$ superconductor phase and its structure is nearly undisturbed by doping of nanoparticles. The scanning electron microscopy images show the improvement in the intergranular links among the superconducting grains with increasing nanoparticles concentration. Microcracks are healed up with the inclusion of these nanoparticles and superconducting volume fraction is also increased. The dielectric properties of these composites strongly depend upon the frequency and temperature. The zero resistivity critical temperature and dielectric properties show opposite trend with the addition of nanoparticles in $Cu_{0.5}Tl_{0.5}Ba_2Ca_2Cu_3O_{10-\delta}$ superconductor matrix.

PACS: **74.70.–b** Superconducting materials other than cuprates;
74.72.–h Cuprate superconductors;
74.62.Bf Effects of material synthesis, crystal structure, and chemical composition;
74.25.Uv Vortex phases (includes vortex lattices, vortex liquids, and vortex glasses).

Keywords: (CuO, CaO_2, and BaO)$_y$/$Cu_{0.5}Tl_{0.5}Ba_2Ca_2Cu_3O_{10-\delta}$ composites, dielectric properties, grain boundaries, microcracks, nanoparticles.

1. Introduction

$(Cu_{0.5}Tl_{0.5})Ba_2Ca_{n-1}Cu_nO_{2n+4-\delta}$ (n = 2, 3, 4, 5, ...) is one of the most important superconductor families in the homologous series of cuprates due to its simple and reproducible ambient pressure synthesis [1]. The compounds of this family have relatively high zero resistivity critical temperature $T_c(R = 0)$, long coherence length along c-axis ξ_c, low superconducting anisotropy $\gamma = \xi_{ab}/\xi_c$, small penetration depth λ, high irreversibility field H_{irr}, higher critical current density J_c, etc. [2]. The performance of these compounds can be affected mainly due to inter-grain voids and pores in their bulk form. Different methods have been tried to minimize the voids and pores in this material [3–16]. Here we adopted a novel approach of CuO, CaO_2, and BaO nanoparticles doping in $Cu_{0.5}Tl_{0.5}Ba_2Ca_2Cu_3O_{10-\delta}$ (CuTl-1223) superconducting matrix to address this issue. The compositional variation at the termination ends of the crystals of $Cu_{0.5}Tl_{0.5}Ba_2Ca_2Cu_3O_{10-\delta}$ superconducting matrix was tried to fix by doping of CuO, CaO_2, and BaO nanoparticles. We have chosen CuO, CaO_2, and BaO nanoparticles for doping due to presence of Cu, Ca, and Ba in the host CuTl-1223 superconducting matrix. We prepared these nanoparticles separately and mixed them in CuTl-1223 superconducting matrix. Therefore, the places where these nanoparticles can sit are only the superconductor grain surfaces and/or between the grains (grain boundaries). The improvement of intergrain connections and microstructures

of (CuO, CaO_2 and $BaO)_y/Cu_{0.5}Tl_{0.5}Ba_2Ca_2Cu_3O_{10-\delta}$ (y = 0, 5, 10, 15%) {(CuO, CaO_2, and $BaO)_y$/CuTl-1223} composites could be expected by the doping of CuO, CaO_2, and BaO nanoparticles in CuTl-1223 superconducting matrix. The main objective of this work is to improve the intergrain connectivity and to investigate its effects on superconductivity as well as on dielectric properties of (CuO, CaO_2, and $BaO)_y$/CuTl-1223 composites.

In CuTl-1223 superconductor, charge carriers are mobile in conducting CuO_2 planes and are static in $Cu_{0.5}Tl_{0.5}Ba_2O_{4-\delta}$ charge reservoir layer. The charge reservoir layer, impurities, voids and grain-boundaries behave as dielectric media, which can be polarized by displacing the charge carriers from their equilibrium position with external applied field. Frequency and temperature dependent dielectric measurements are of great importance to study the induced dipolar polarization in these composites for their dielectric properties [17,18]. In this article we report the frequency and temperature dependent dielectric measurements of (CuO, CaO_2, and $BaO)_y$/CuTl-1223 composites. The dielectric measurements at different temperatures starting from room temperature to superconducting state temperature can be significant for understanding of the mechanism of the superconductivity in these composites.

There are four types of polarization depending upon the frequency of applied external field.

(i) Electronic polarization, observed in the frequency of the order of ~ 10^{15} Hz.

(ii) Atomic and ionic polarization is observed in the range from 10^{10} to 10^{13} Hz.

(iii) The dipolar or oriental polarizations are observed in the sub-infrared frequency range from 10^3 to 10^6 Hz. The dipolar polarizations play main role in the dielectric properties of these composites.

(iv) The interfacial polarizations are usually observed in the low frequency range of the order of ~ 10^3 Hz and can extend to a frequency of few kHz [19,20].

There are few reports available in the literature on the dielectric measurements of oxides of the high temperature superconductors in which giant dielectric constants are observed [17,21,22].

2. Experimental

The bulk ceramic CuTl-1223 superconductor is synthesized by solid-state reaction accomplished in two stages. At the first stage $Cu_{0.5}Ba_2Ca_2Cu_3O_{10-\delta}$ precursor material is prepared by using $Ba(NO_3)_2$, $Ca(NO_3)_2$, Cu(CN) as starting compounds. These compounds are mixed and ground in appropriate ratios in an agate mortar and pestle. Thoroughly mixed material is heated in chamber furnace at 860 °C for 24 h followed by furnace cooling to room temperature. The precursor material is mixed with Tl_2O_3 and then ground again for one hour to get CuTl-1223 superconductor composition. The nanoparticles of CuO, CaO_2 and BaO are synthesized by co-precipitation method separately and then these nanoparticles are added by wt% in CuTl-1223 superconductor matrix. The powder obtained is pelletized under 3.8 tons/cm^2 pressure and pellets are wrapped in gold capsules for sintering. The pellets in gold capsules are sintered at 860 °C for 10 min in preheated chamber furnace followed by quenching to room temperature to get (CuO, CaO_2, and $BaO)_y$/CuTl-1223 (y = 0, 5%, 10%, and 15%) as final composition. The post-annealing experiments on these composites are carried out in flowing oxygen at 550 °C for 6 h in a tubular furnace.

The structure of the material is determined by x-ray diffraction (XRD) scan (D/Max IIIC Rigaku with a CuK_α source of wavelength 1.54056 Å) and cell parameters are calculated by using a computer program. The conventional four-probe technique is used for dc-resistivity measurements and the value of current during the measurements is kept 1 mA. The dc-resistivity measurement is carried out during the heating cycle from 78 K to room temperature, i.e., nearly 300 K. The rate of heating is kept 1 to 3 K/min during these measurements. The frequency dependent dielectric measurements are performed with the help of Hewlett-Packard 4275A Multi-Frequency LCR Meter in the frequency range from 10 kHz to 10 MHz. The conventional two-probe technique was used for the dielectric measurements. Silver paint is applied to both the surfaces of the sample and is dried at room temperature. The electrical connections of thin copper wires on silver electrode surfaces are made with the help of silver paint. By measuring the capacitance C and conductance G, the dielectric constants (ε_r' and ε_r''), dielectric loss (tan δ) and ac-conductivity (σ_{ac}) of the samples are calculated using the following expressions [17].

$$\varepsilon_r' = Cd/A\varepsilon_0, \quad (1)$$

$$\varepsilon_r'' = Gd/\omega A\varepsilon_0, \quad (2)$$

$$\tan\delta = \varepsilon_r'/\varepsilon_r'', \quad (3)$$

$$\sigma_{ac} = \omega\varepsilon_0\varepsilon_r'\tan\delta, \quad (4)$$

where $\omega = 2\pi f$ and f is the frequency of applied ac-field, d is the thickness of the pellet (m), ε_0 is the permittivity of free space ($\varepsilon_0 = 8.85\cdot10^{-12}$ F/m) and A is the area of the electrode (m^2).

3. Results and discussion

The x-ray diffraction (XRD) scans of (CuO, CaO_2, and $BaO)_y$/CuTl-1223 composites with 0, 5%, and 10% by wt% of CuO, CaO_2 and BaO nanoparticles are shown in Fig. 1. Most of the diffraction peaks are indexed according to CuTl-1223 tetragonal structure following the *P4/mmm* space group and calculated unit cell parameters are a = = 3.80 Å and c =14.95 Å for y = 0, a = 3.79 Å and c = 15.00 Å for y = 5% and a = 3.78 Å and c = 15.01 Å for y = 10%, respectively. Few unindexed peaks of very low intensity represent the presence of very small amount of impurities or some other phases. This shows that the addi-

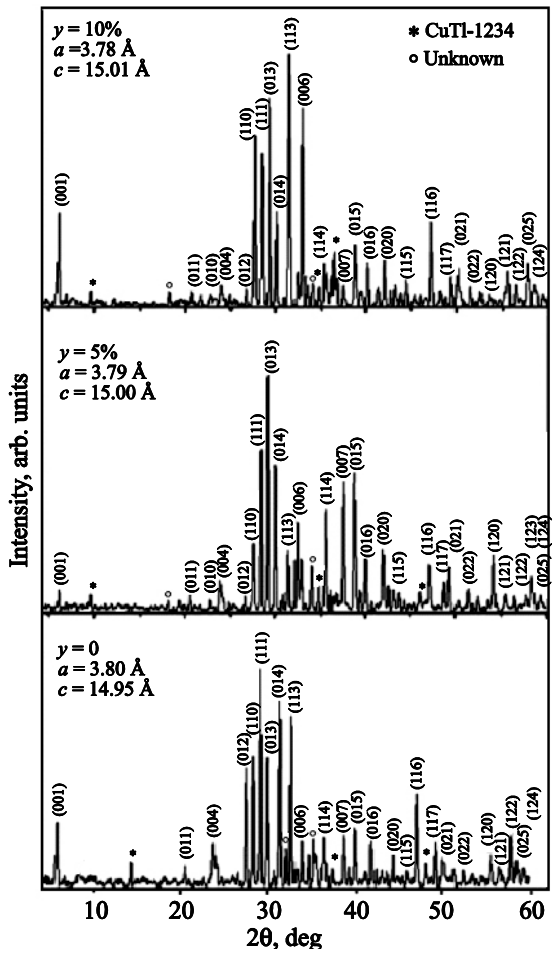

Fig. 1. X-ray diffraction patterns of (CuO, CaO_2, and $BaO)_y$/CuTl-1223 composites for different *y*.

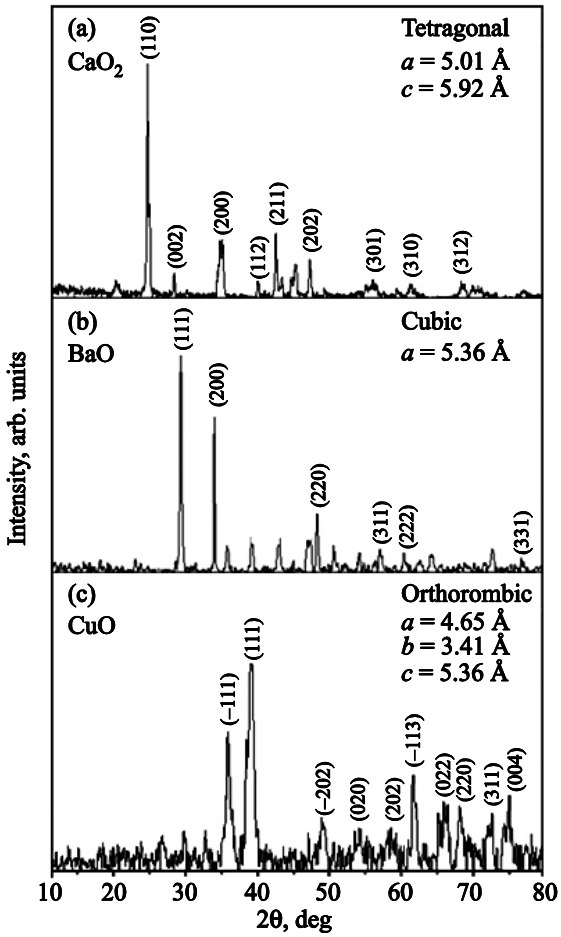

Fig. 2. X-ray diffraction patterns of CaO_2 nanoparticles (a), BaO nanoparticles (b), CuO nanoparticles (c).

tion of nanoparticles has not changed the stoichiometry of the final compound. This gives us a clue that nanoparticles remain at the intergrain boundaries of CuTl-1223 superconductor matrix used only to heal up the intergrain voids. The XRD scans of CaO_2, BaO and CuO nanoparticles are shown in Fig. 2. All the indexed peaks in the XRD graphs correspond to CaO_2, BaO and CuO structure. However, there are some unknown peaks present in all the XRD patterns which may be due the presence of impurities in the precursors (chemicals). The tetragonal structure is observed for CaO_2 nanoparticles with unit cell parameters $a = 5.01$ Å, $c = 5.92$ Å and unit cell volume = $148.6 \cdot 10^{-3}$ nm^3. The cubic structure is observed for BaO nanoparticles with $a = 5.36$ Å and unit cell volume = $153.6 \cdot 10^{-3}$ nm^3. The CuO nanoparticles have orthorhombic structure with $a = 4.65$ Å, $b = 3.41$ Å, $c = 5.36$ Å and unit cell volume = $84.97 \cdot 10^{-3}$ nm^3. The average particle size of CaO_2, BaO, and CuO nanoparticles calculated by using Debye–Scherrer formula is about 33, 72 and 17 nm, respectively.

The resistivity versus temperature measurements of (CuO, CaO_2, and $BaO)_y$/CuTl-1223 composites are shown in Fig. 3. These measurements show the metallic variations in resistivity from room temperature down to onset of superconductivity. The room temperature resistivity varies from 1.5 to 6.3 Ω·cm and zero resistivity critical temperature $T_c(R = 0)$ increases from 87 to 97–99 K after doping

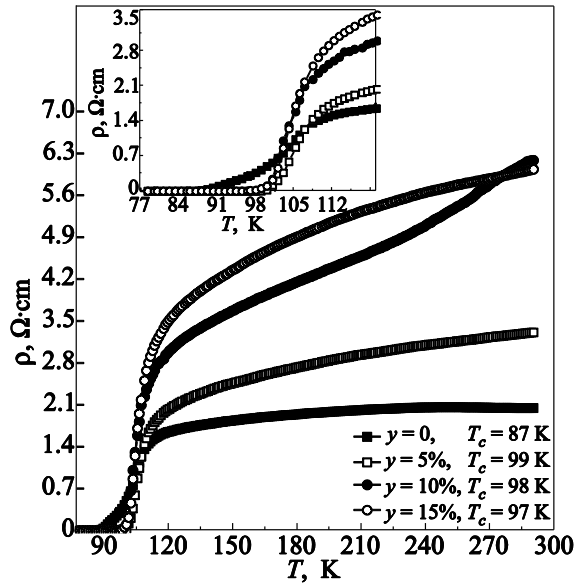

Fig. 3. Resistivity vs temperature measurement of (CuO, CaO_2, and $BaO)_y$/CuTl-1223 ($y = 0$, 5%, 10%, 15%) composites.

of CuO, CaO_2, and BaO nanoparticles in CuTl-1223 superconductor matrix. The increase in $T_c(R = 0)$ is due to improved bulk superconductivity after incorporation of these nanoparticles.

Fourier transform infrared spectroscopy (FTIR) is very sensitive technique used to detect a trace amount of impurity in the material. The FTIR absorption measurement of (CuO, CaO_2, and BaO)$_y$/CuTl-1223 composites with 0, 5%, 10%, and 15% of CuO, CaO_2 and BaO nanoparticles are shown in Fig. 4. In these samples the apical oxygen mode of types Cu(1)–O_A–Cu(2) and Tl–O_A–Cu(2) are found to be around 545 and 445 cm^{-1}, the planer oxygen mode of types Cu(2)–O_p–Cu(2) around 573 cm^{-1} and O_δ mode in charge reservoir layer around 695 cm^{-1}. The positions of these modes for all samples remained almost same. The same position of these modes gives us evidence that there is no change in the stoichiometery of the interagrain material with the addition of CuO, CaO_2 and BaO nanoparticles.

The scanning electron micrographs (SEM) of (CuO, CaO_2, and BaO)$_y$/CuTl-1223 composites with y = 0, 5%, 10% and 15% are shown in Fig. 5. These SEM pictures indicate the significant reduction of intergrain voids in the samples after addition of nanoparticles. The similar atoms (Cu, Ca, and Ba) between the superconducting grains and nanoparticles interact at the superconductor/nanoparticle interface and results in the improvement of the intergranular coupling and superconductor properties.

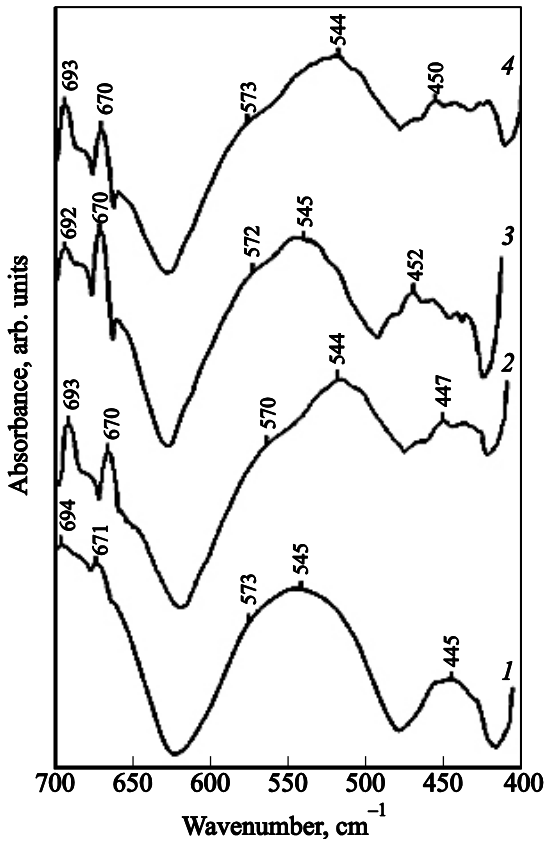

Fig. 4. Fourier transform infrared (FTIR) spectra of (CuO, CaO_2, and BaO)$_y$/CuTl-1223 composites, y, %: 0 (*1*), 5 (*2*), 10 (*3*), 15 (*4*).

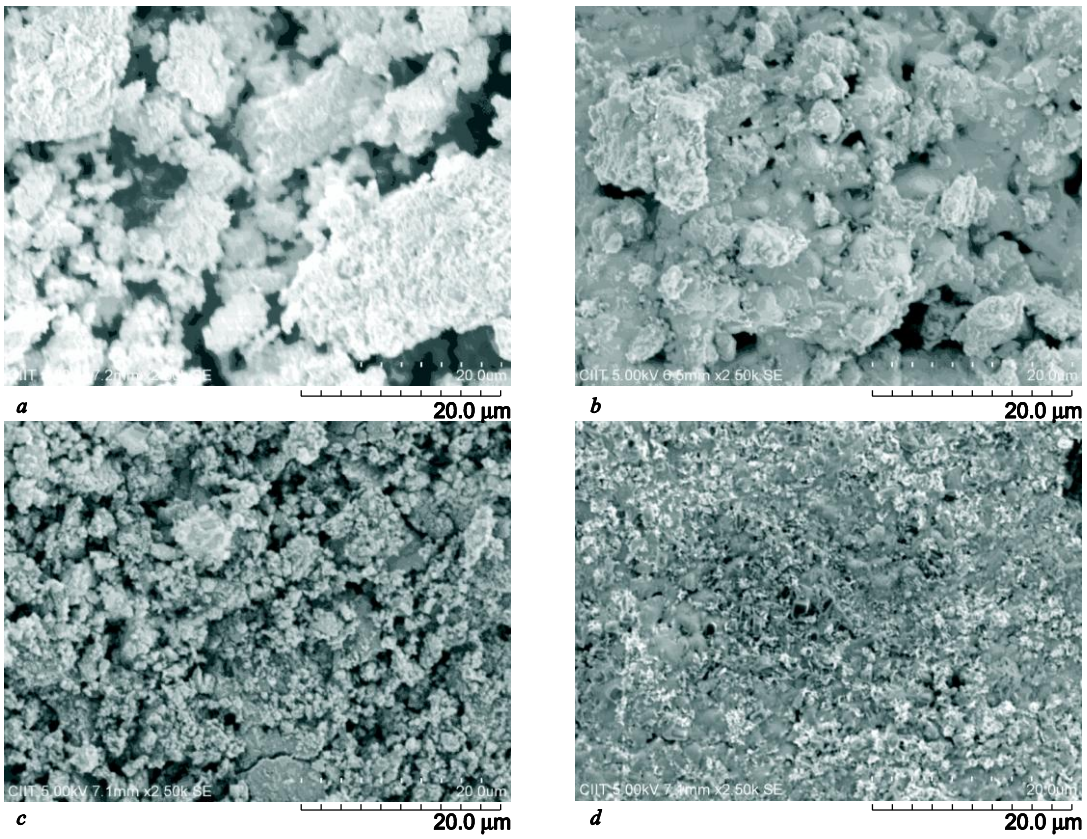

Fig. 5. Scanning electron micrographs of (CuO, CaO_2, and BaO)$_y$/CuTl-1223 composites, y, %: 0 (a), 5 (b), 10(c), 15 (d).

We also investigated the dielectric properties of the composites to compare with the undoped CuTl-1223 superconductor. The variation in the frequency dependent real part of dielectric constant (ε_r') of CuTl-1223 samples at various temperatures and frequencies is shown in Fig. 6. The real part of dielectric constant (ε_r') gives the part of energy stored in the material when it is exposed to applied external electric field. The maximum value of ε_r' varies from $-1.57\cdot10^{14}$ to $-1.78\cdot10^{14}$ in undoped CuTl-1223 superconductor at 10 kHz by varying the measurement temperature from 78 to 300 K. The value of ε_r' decreases gradually with the doping of CuO, CaO_2 and BaO nanoparticles in CuTl-1223 superconducting matrix. The maximum value of ε_r' varies from $-7.9\cdot10^{13}$ to $-9.16\cdot10^{13}$, $-7.04\cdot10^{13}$ to $-7.93\cdot10^{13}$, and $-6.03\cdot10^{13}$ to $-6.75\cdot10^{13}$ in (CuO, CaO_2, and BaO)$_y$/CuTl-1223 composites with 0, 5%, 10% and 15% of CuO, CaO_2, and BaO nanoparticles at 10 kHz by varying the measurement temperature from 78 to 300 K, respectively. The most possible reasons for gradual decrease in ε_r' after doping of CuO, CaO_2, and BaO nanoparticles in (CuO, CaO_2, and BaO)$_y$/CuTl-1223 composites may be the increase of volume fraction of main phase, improved inter-grain connectivity due to healing up of microcracks, improved microstructure of samples, and comparative decrease in impurities [23]. At higher frequencies the time period of oscillation of the applied field is too fast as compared to the characteristic time of dipolar polarization, therefore, ε_r' decreases rapidly [24]. So the decrease of ε_r' is due to reduction of dipolar polarization in the material. Therefore, it can be suggested that dielectric constant mainly originates from electronic as well as from lattice polarization in (CuO, CaO_2, and BaO)$_y$/CuTl-1223 composites. The decrease of ε_r' with the increase of temperature can be related to the decrease of polarizability in (CuO, CaO_2, and BaO)$_y$/CuTl-1223 composites with the increase of temperature.

The imaginary part of dielectric constant (ε_r'') under the applied external electric field gives us information about the absorption of energy throughout the interfaces. The interfaces consist of grain boundaries, localized defects, and localized charge densities at the defects sites in the materials. More absorption of energy is observed in (CuO, CaO_2, and BaO)$_y$/CuTl-1223 composites at 300 K and 10 kHz as shown in Fig. 7. The maximum values of ε_r'' vary around $1.06\cdot10^9$ to $1.18\cdot10^9$, $5.33\cdot10^8$ to $6.09\cdot10^8$, $3.82\cdot10^8$ to $5.37\cdot10^8$, and $4.02\cdot10^8$ to $4.45\cdot10^8$ for 0, 5%, 10% and 15% by wt% doping in (CuO, CaO_2, and BaO)$_y$/CuTl-1223 composites at 10 kHz by varying the measurement temperature from 78 to 300 K, respectively. The Maxwell–Wagner model and Koop's phenomenological theory help us to understand the phenomena of dielectric dispersion [25,26]. In these models, a dielectric medium has been assumed to be made up of well conducting grains separated by low conducting grain boundaries. The grains have high values of permittivity due to highly conductive nature as compared to that of poorly conducting grain boundaries. Therefore, at lower frequencies the grain boundaries are more effective than electrical conducting grains.

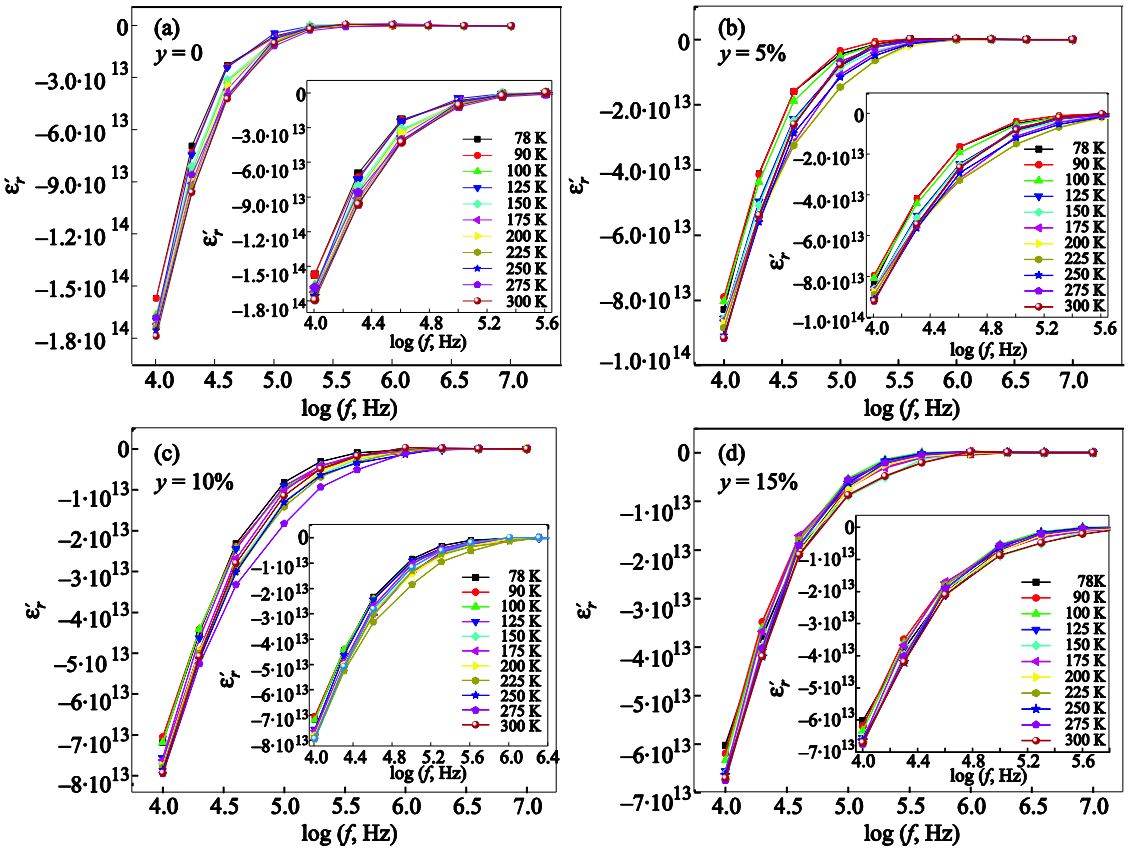

Fig. 6. (Color online) Dielectric constant ε_r' vs log of frequency of (CuO, CaO_2, and BaO)$_y$/CuTl-1223 composites for different *y*.

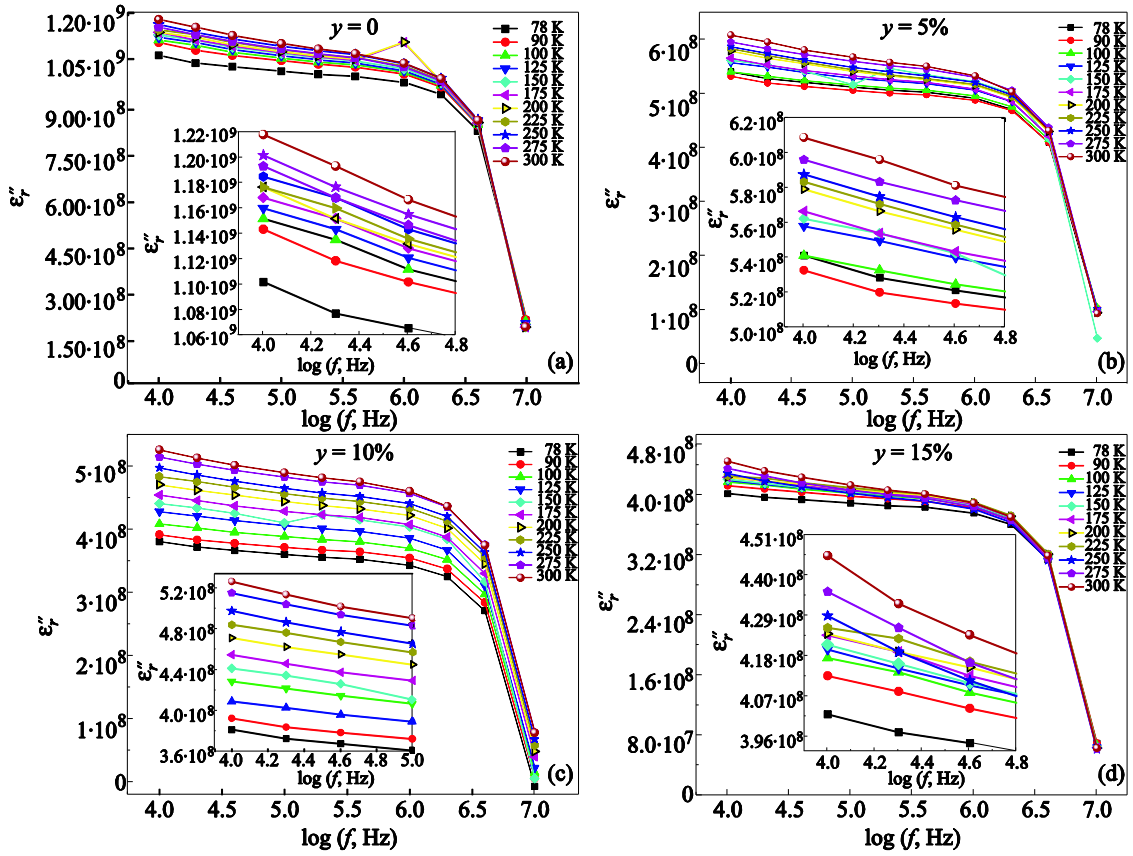

Fig. 7. (Color online) The imaginary part of dielectric constant (ε_r'') vs log of frequency of (CuO, CaO_2, and BaO)$_y$/CuTl-1223 composites for different *y*.

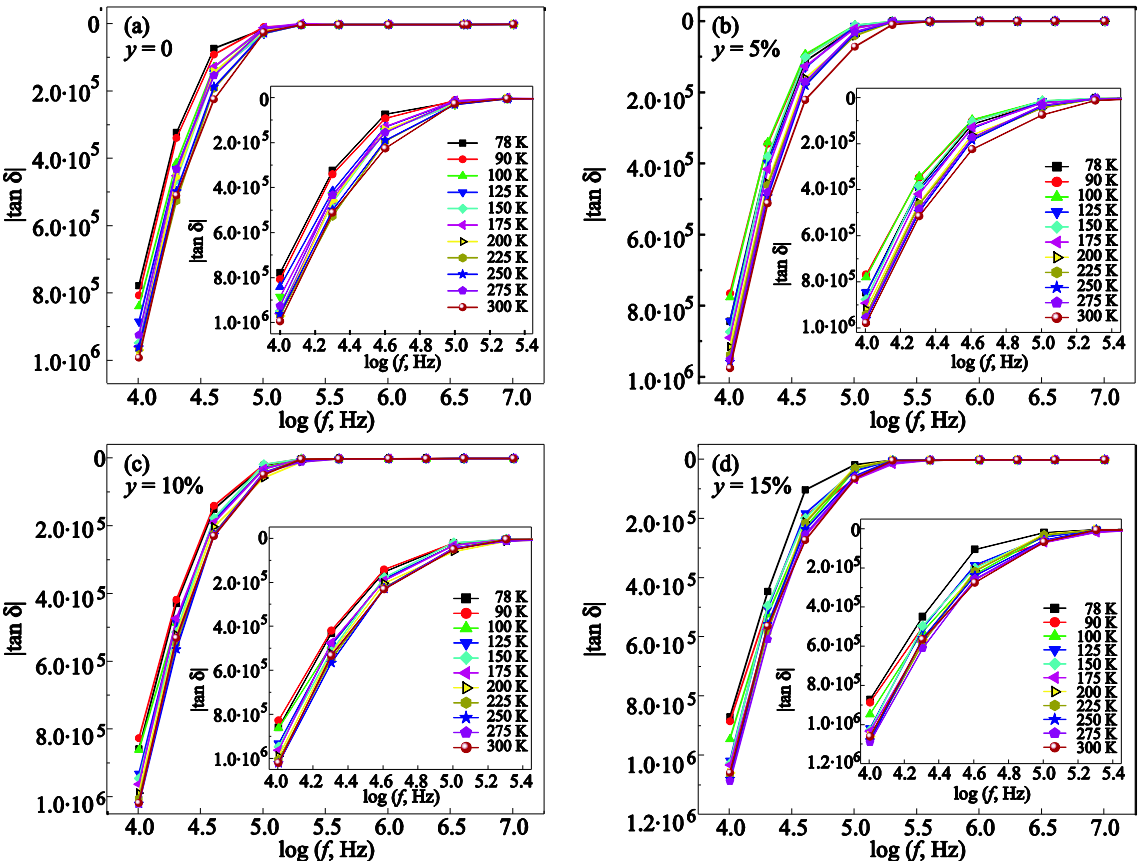

Fig. 8. (Color online) The absolute dielectric loss |tan δ| vs log of frequency of (CuO, CaO_2, and BaO)$_y$/CuTl-1223 composites for different *y*.

The ratio of energy dissipated per radian in the material to the energy stored determines the dielectric loss factor (tan δ) and its absolute value for (CuO, CaO_2, and BaO)$_y$/CuTl-1223 composites are shown in Fig. 8. A relative increase in the value of |tan δ| is observed in (CuO, CaO_2, and BaO)$_y$/CuTl-1223 composites after nanoparticle doping at higher frequency. The values of |tan δ| are in the range of $7.76\cdot10^5$ to $9.91\cdot10^5$, $7.73\cdot10^5$ to $9.75\cdot10^5$, $8.24\cdot10^5$ to $1.01\cdot10^6$, and $8.68\cdot10^5$ to $1.09\cdot10^6$ for (CuO, CaO_2, and BaO)$_y$/CuTl-1223 composite with y = 0, 5%, 10%, and 15%, at 10 kHz by varying measurement temperature from 78 to 300 K, respectively.

The ac-conductivity (σ_{ac}) of (CuO, CaO_2, and BaO)$_y$/CuTl-1223 composites are shown in Fig. 9. The maximum value of σ_{ac} changes in the range $2.25\cdot10^{-5}$ to $2.61\cdot10^{-5}$, $2.65\cdot10^{-5}$ to $3.09\cdot10^{-5}$, $2.73\cdot10^{-5}$ to $3.87\cdot10^{-5}$, and $6.09\cdot10^{-5}$ to $6.93\cdot10^{-5}$ for (CuO, CaO_2, and BaO)$_y$/CuTl-1223 composite with y = 0, 5%, 10%, and 15%, at 10 kHz by varying measurement temperature from 78 to 300 K, respectively. The value of σ_{ac} increases with doping of CuO, CaO_2, and BaO nanoparticles in CuTl-1223 superconducting matrix and the most possible reason is the improved intergrain connectivity due to healing up of microcracks. The ac-conductivity (σ_{ac}) may arise from free as well as bound carriers. When the ac-conductivity (σ_{ac}) increases with increase of frequency then it will be due to bound carriers trapped in the sample but when it decreases with the increase of frequency then it will be due to mobile free carriers [24].The value of σ_{ac} becomes zero for all the samples in the high frequency range at all temperatures, which shows its independence of temperature at high frequencies. But in the low frequency range the value of σ_{ac} increases systematically as the frequency decreases but its dependence upon temperature in low frequency range is also not significant. The variation of σ_{ac} with frequency and its almost independence of temperature can be very useful feature of these composites for application point of view.

4. Conclusion

The population of voids and pores is decreased by doping of CuO, CaO_2, and BaO nanoparticles and textured crystalline material is obtained. The addition of nanoparticles increased the superconducting volume fraction of the samples by improving the intergrain connectivity and by healing up of microcracks in the samples. The gradual decrease of ε_r' with the addition of CuO, CaO_2, and BaO nanoparticles is due to the effect of these nanoparticles in increasing the volume fraction of main phase, healing up of microcracks, increasing the intergrain connectivity, improving the microstructure of samples and decreasing the impurities and electrical inhomogeneity. The ac-conductivity (σ_{ac}) of (CuO, CaO_2, and BaO)$_y$/CuTl-1223 compo-

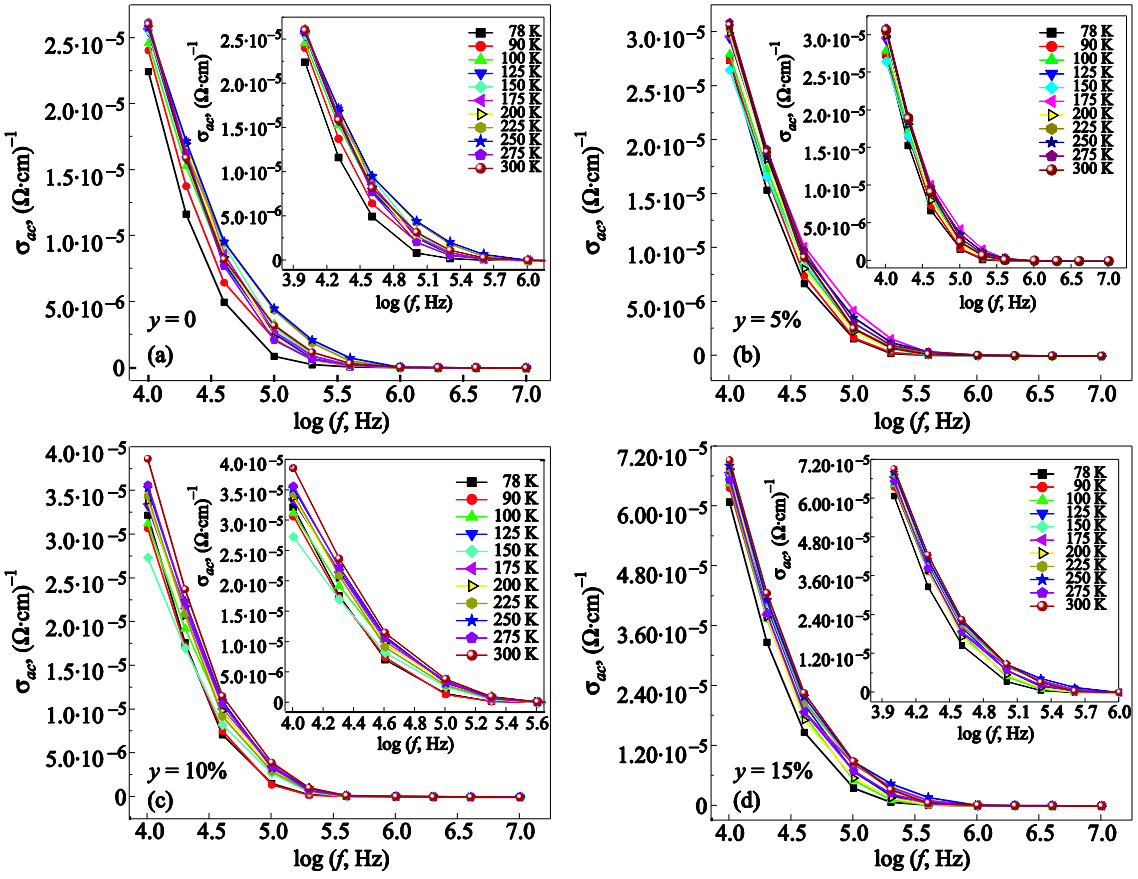

Fig. 9. The ac-conductivity σ_{ac} vs log of frequency of (CuO, CaO_2, and BaO)$_y$/CuTl-1223 composites for different y.

sites increases gradually with the increase of doping percentage of nanoparticles. As the value of σ_{ac} decreases with the increase of frequency, therefore, the conduction mechanism is due to translation of free carriers in the material.

1. H. Yamamoto, K. Tanaka, K. Tokiwa, H. Hirabayashi, M. Tokumoto, Nawazish A. Khan, and H. Ihara, *Physica C* **302**, 137 (1998).
2. H. Ihara, *Physica C* **364–365**, 289 (2001).
3. K. Tanaka, A. Iyo, N. Terada, K. Tokiwa, S. Miyashita, Y. Tanaka, T. Tsukamoto, S.K. Agarwal, T. Watanabe, and H. Ihara, *Phys. Rev. B* **63**, 064508-6 (2001).
4. K. Tanaka, A. Iyo, Y. Tanaka, K. Tokiwa, M. Tokumoto, M. Ariyama, T. Tsukamoto, T. Watanabe, and H. Ihara, *Physica B* **284–288**, 1081 (2000).
5. T. Watanabe, S. Miyashita, N. Ichioka, K. Tokiwa, K. Tanaka, A. Iyo, Y. Tanaka, and H. Ihara, *Physica B* **284–288**, 1075 (2000).
6. K. Tokiwa, H. Aota, C. Kunugi, K. Tanaka, Y. Tanaka, A. Iyo, H. Ihara, and T. Watanabe, *Physica B* **284–288**, 1077 (2000).
7. K. Tanaka, A. Iyo, Y. Tanaka, K. Tokiwa, N. Terada, M. Tokumoto, M. Ariyama, T. Tsukamoto, S. Miyashita, T. Watanabe, and H. Ihara, *Physica B* **284–288**, 1079 (2000).
8. H. Ihara, K. Tanaka, Y. Tanaka, A. Iyo, N. Terada, M. Tokumoto, M. Ariyama, 1. Hase, A. Sundaresan, N. Hamada, S. Miyashita, K. Tokiwa, and T. Watanabe, *Physica C* **341–348**, 487 (2000).
9. H. Ihara, K. Tanaka, Y. Tanaka, A. Iyo, N. Terada, M. Tokumoto, F. Tateai, M. Kawamura, K. Ishida, S. Miyashita, and T. Watanabe, *Physica B* **284–288**, 1085 (2000).
10. H. Ihara, A. Iyo, K. Tanaka, K. Tokiwa, K. Ishida, N. Terada, M. Tokumoto, Y. Sekita, T. Tsukamoto, T. Watanabe, and M. Umeda, *Physica C* **282**, 1973 (1997).
11. A.A. Khurram and Nawazish A. Khan, *Supercond. Sci. Technol.* **19**, 679 (2006).
12. Nawazish A. Khan, G. Husnain, and K. Sabeeh, *J. Phys. Chem. Solids* **67**, 1841(2006).
13. M. Mumtaz and Nawazish A. Khan, *Fiz. Nizk. Temp*. **36**, 196 (2010) [*Low Temp. Phys.* **36**, 154 (2010)].
14. Nawazish A. Khan and Safeer Husnain, *J. Alloys Compd.* **475**, 652 (2009).
15. P.E. Kazin, M. Jansen, A. Larrea, G.F. De la Fuente, and Yu.D. Tretyakov, *Physica C* **253**, 391 (1995).
16. P. Majewski, S. Elschner, B. Hettich, C. Lang, S. Kaescheand, and F. Aldinger, *Supercond. Sci. Technol.* **7**, 514 (1994).
17. S. Cavdar, H. Koralay, N. Tugluoglu, and A. Gunen, *Supercond. Sci Technol.* **18**, 1204 (2005).
18. J.B. Shi, Y. Hsu, and C.T. Lin, *Physica C* **299**, 272 (1998).
19. M.S. Vijaya and G. Rangarajan, *Materials Science*, Tata McGraw-Hill Publishing Company Limited, New Delhi India (2004).
20. L.L. Hench and J.K. West, *Principles of Electronic Ceramics*, Wiley, New York (1990).
21. Xiaofeng Xu, Zhengkuan Jiao, Minyi Fu, Lixin Feng, Kaixun Xu, Rongqing Zuo, and Xuezhi Chen, *Physica C* **417**, 166 (2005).
22. R.K. Nkum, M.O. Gyekye, and F. Boakye, *Solid. State Commun.* **122**, 569 (2002).
23. Nawazish A. Khan, Abida Saleem, and S. Tajammul Hussain, *J. Supercond. Nov. Magn.* **25**, 1725 (2012).
24. N.H. Mohammed, *J. Supercond. Nov. Magn.* **25**, 45 (2012).
25. J.C. Maxwell, *Electricity and Magnetism*, Oxford Univ. Press, Oxford (1892), Vol. 1, Sect. 328.
26. C.G. Koops, *Phys. Rev*. **83**, 121 (1951).